Editors' Suggestion

Kondo effect in ferromagnetic quantum critical $CeRh_6Ge_4$

Martin Sundermann,[1,2] Joe D. Thompson,[3,*] Eric D. Bauer,[3] Chun-Fu Chang,[1] Sheng-Huai Chen,[1] Chang-Yang Kuo,[4,5] Liu Hao Tjeng,[1] Gertrud Zwicknagl,[6,1] and Andrea Severing[1,†]

[1]*Max Planck Institute for Chemical Physics of Solids, Nöthnitzer Straße 40, 01187 Dresden, Germany*
[2]*PETRA III, Deutsches Elektronen-Synchrotron DESY, Notkestraße 85, 22607 Hamburg, Germany*
[3]*Los Alamos National Laboratory, Los Alamos, New Mexico 87545, USA*
[4]*Department of Electrophysics, National Yang Ming Chiao Tung University, Hsinchu 30010, Taiwan*
[5]*National Synchrotron Radiation Research Center, 101 Hsin-Ann Road, Hsinchu 300092, Taiwan*
[6]*Institute for Mathematical Physics, Technische Universität Braunschweig, 38106 Braunschweig, Germany*

(Received 20 March 2026; revised 4 June 2026; accepted 9 June 2026; published 29 June 2026)

The mechanism of a pressure-induced quantum critical point in the heavy fermion ferromagnet $CeRh_6Ge_4$ has attracted interest, as ferromagnetic quantum criticality in a clean itinerant Ce compound is typically avoided. The localized versus itinerant character of the $4f$ electrons is a key aspect for understanding this behavior. We investigated the electronic structure of the $4f$ shell in $CeRh_6Ge_4$ using core-level photoelectron and x-ray absorption spectroscopy, demonstrating the hybridization of Ce $4f$ with the conduction electrons. Linearly polarized x-ray absorption reveals a temperature-dependent linear dichroism consistent with the crystal-electric-field sequence as inferred from the static susceptibility. This dichroism cannot be described by an ionic full-multiplet model alone, but is reproduced by including the Kondo effect within a single-impurity Anderson model in the noncrossing approximation. The Kondo effect mixes higher-lying crystal-field states into a resulting multiorbital ground state with $4f$ occupancy, $n_f \sim 0.9$. Deviations at low temperatures between the measured linear dichroism and calculated dichroism suggest an orbital-dependent Kondo effect. A scenario in which there is a multiorbital ground state and orbital-dependent Kondo hybridization should be a starting point for a model of pressure-induced criticality in $CeRh_6Ge_4$.

DOI: 10.1103/6w55-56wk

I. INTRODUCTION

Ferromagnetic (FM) quantum critical points (QCPs) in clean itinerant Kondo materials are usually avoided, preempted either by first-order phase transitions or by the formation of inhomogeneous magnetic phases [1–6]. The metallic compound $YbNi_4P_2$ undergoes a FM quantum phase transition upon substitution of As on the P sites; however, such substitution also introduces disorder [7]. In contrast, stoichiometric $CeRh_6Ge_4$ orders ferromagnetically at $T_C = 2.5$ K [8,9] out of a strongly correlated paramagnetic state and exhibits a FM QCP under external pressure at $p_c = 0.8$ GPa. Moreover, at its QCP the material displays strange-metal behavior—a logarithmic divergence of specific heat divided by temperature and linear-in-temperature resistivity [10,11], which commonly occurs in quantum-critical antiferromagnets [12]. Theoretically, a FM QCP in a *clean* material can arise in itinerant ferromagnets if the system is quasi-one-dimensional [6,13] or if there is strong antisymmetric spin-orbit coupling due to broken inversion symmetry [6,14,15]. If, however, magnetic electrons are localized in a Kondo lattice, criticality could arise from a breakdown of the Kondo effect at the QCP, producing a change in Fermi volume from small to large for coherent quasiparticles [11,13]. A change in Fermi surface would also be consistent with overdamped phase fluctuations of hybridization that could account for both ferromagnetic criticality and strange metal behaviors [16]. Each of these scenarios has been invoked to account for criticality in $CeRh_6Ge_4$ [11,14,16–20], which emphasizes the conundrum it poses. The distinguishing characters of these scenarios is the nature of the $4f$ electron and the role played by the Kondo effect. Clarifying these characters is a necessary step toward resolving the conundrum.

$CeRh_6Ge_4$ crystallizes in the hexagonal $LiCo_6P_4$-type structure ($P\bar{6}m2$) without an inversion center [8]. The structure consists of Ce-Rh1-Ge1 and Rh2-Ge2 layers, with triangular lattices of Ce stacked along the c-axis, giving rise to chains of Ce along this direction. Ce occupies the 1a sites with D_{3h} point symmetry, in which Ce ions experience a hexagonal ($\bar{6}m2$) crystal-electric field (CEF) that splits the $J = 5/2$ multiplet into three Kramers doublets, each corresponding to a pure j_z state ($|\pm 1/2\rangle$, $|\pm 3/2\rangle$, $|\pm 5/2\rangle$).

The magnetic properties of $CeRh_6Ge_4$ are very anisotropic, with the crystallographic c direction being the hard axis, thus restricting the ordered moments to the ab plane. The effective moment μ_{eff} amounts to $2.35\mu_B$/Ce, which is close to the

*Contact author: jdt@lanl.gov
†Contact author: andrea.severing@cpfs.mpg.de

Published by the American Physical Society under the terms of the Creative Commons Attribution 4.0 International license. Further distribution of this work must maintain attribution to the author(s) and the published article's title, journal citation, and DOI. Open access publication funded by Max Planck Society.

full Ce^{3+} moment, and the ordered moments as determined from magnetization [11], muon spin resonance (μSR) [21], and nuclear quadrupole resonance (NQR) [22] are of the order of $0.2 - 0.3\,\mu_B$/Ce. This is much smaller than the in-plane expectation value of $1.28\,\mu_B$/Ce for the $|\pm 1/2\rangle$ CEF ground state. Because $|\pm 1/2\rangle$ is the only state that corresponds to a finite in-plane moment, it is deduced to be a ground state. Fits to the anisotropy of the static susceptibility yield the $|\pm 3/2\rangle$ CEF state 5.8 meV and the $|\pm 5/2\rangle$ CEF state at 22.1 meV [21].

Angle-dependent quantum oscillation measurements at ambient pressure indicate that $CeRh_6Ge_4$ is a *clean* material, and they are more consistent with band-structure calculations that assume that the $4f$ electrons do not contribute to the Fermi surface at ambient pressure. This suggests that $CeRh_6Ge_4$ does not form a coherent Fermi liquid and that Kondo-breakdown criticality may be relevant for a description of quantum criticality in $CeRh_6Ge_4$ [17].

Alternatively, the small ordered moment [11,21,22], the large Sommerfeld coefficient ($\sim$250 mJ/mol K^2) deep in the ordered state, and the small fraction of entropy (about 20% of $R \ln 2$) released at the ordering transition [9] are more indicative of a local Fermi liquid and a substantial Kondo effect. This is consistent with inelastic neutron scattering results, which reveal a broad quasielastic linewidth of 3.3 meV ($\approx$40 K) and a strongly broadened inelastic response [21], as well as with angle-resolved photoelectron spectroscopy (ARPES) that reveals dispersive $4f$ bands and anisotropic hybridization between $4f$ and conduction electrons well above T_C [18]. In fact, the Kondo-derived peak observed in ARPES persists to temperatures well above both the Kondo temperature $T_K \sim 20$ K estimated from entropy [9], and the coherence temperature estimated from resistivity, $T^* \sim 80$ K [18]. Thermopower measurements question a Kondo-breakdown scenario with fully localized moments [19]. Instead, the results of these measurements [19] argue that the conditions for quantum criticality of itinerant ferromagnetism are fulfilled due to the formation of a quasiquartet ground state arising from the intermixing of CEF states in the presence of the Kondo effect. They further propose that orbital selective hybridization, supported by ARPES [18], may reconcile the discrepancies among the various experimental findings.

From Ce $3d$ core-level photoelectron spectroscopy (PES) and $M_{4,5}$ edges polarized x-ray absorption spectroscopy (XAS), we address two outstanding questions posed by $CeRh_6Ge_4$: what is the nature of its $4f$ electrons, and what is an appropriate description of its crystal-field excitations? Satellites in the core-level PES provide insight into the presence of Kondo coupling and the associated configurational mixing. At low temperatures, linearly polarized XAS gives access to the orbital occupation of the $4f$ shell ground state and allows us to probe possible mixing of excited CEF states into the ground state induced by the Kondo effect.

II. METHOD: EXPERIMENT AND ANALYSIS

$CeRh_6Ge_4$ single crystals were grown with the Bi-flux technique as described by Vosswinkel *et al.* [8]. X-ray diffraction pattern confirmed the $P6m2$ hexagonal structure with lattice constants $a = 7.15$ Å and $c = 3.85$ Å. Magnetic susceptibility and magnetization measurements performed in an MPMS3 magnetometer (Quantum Design) gave a ferromagnetic transition at 2.5 K and agreement with previously reported magnitude and anisotropy of magnetic properties of $CeRh_6Ge_4$ [9,11,21].

PES and XAS measurements were performed at the NSRRC-MPI TPS-45A1 endstation at the Taiwan Photon Source (TPS) with a beam focus of $V \times H = 25\,\mu\text{m} \times 30\,\mu\text{m}$. Crystals of $CeRh_6Ge_4$ were cleaved *in situ* under ultrahigh-vacuum (UHV) conditions of $p < 10^{-10}$ mbar to ensure a clean surface.

PES was measured at 200 K with horizontally polarized light at a fixed photon energy of 1260 eV. The photoelectrons were detected with an MBS A-1 analyzer with a lens-4 detector, placed at an angle of 120° between photon and electron wave vectors in the horizontal plane. The energy resolution was 175 meV as measured on a Pt reference with the Fermi energy at 1256.3 eV. A polynomial correction was applied to straighten the spectrum prior to subtracting a Shirley-type background.

XAS measurements at the Ce $M_{4,5}$ edges were performed in the total-electron-yield (TEY) mode with linearly polarized light and an energy resolution of about 100 meV. All spectra were normalized to the incident photon flux, calibrated in energy to a CuO reference, and background-subtracted using the preedge intensity. The single crystal was aligned such that the electric field vector $\vec{E}$ was either perpendicular to the crystallographic c axis ($\vec{E} \perp c$) or approximately parallel to it ($\vec{E} \parallel \tilde{c}$, with $\tilde{c}$ 20° off c, due to geometric restrictions). The presented $\vec{E} \parallel c$ spectra are corrected for this offset, as described in Appendix A.

Core-level PES spectra were analyzed using full-multiplet (fm) configuration-interaction (CI) calculations performed with the Quanty code [23]. The model includes a single, energetically degenerate ligand shell hybridizing equally with all $4f$ states, preserving spherical symmetry [24], and was restricted to the $4f^0$, $4f^1\underline{L}$, and $4f^2\underline{\underline{L}}$ configurations. Here $\underline{L}$ and $\underline{\underline{L}}$ denote the number of ligand holes. Atomic spin-orbit coupling values from the Cowan code [25] were used for both $4f$ and $3d$ shells, while Coulomb interactions, starting with the Cowan values, were reduced to 60% ($4f$-$4f$) and 80% ($3d$-$4f$) to account for screening effects within the solid [26,27]. The spectral lines are broadened using a combination of Gaussian (FWHM = 1.1 eV) and Lorentzian (FWHM = 1.4 eV) functions to account for instrumental resolution and lifetime broadening. Additionally, a Mahan function is applied to capture the asymmetry of the line shapes (cutoff parameter $\xi_M = 4$ eV, asymmetry factor $\alpha_M = 0.15$) (see, e.g., Ref. [28]). The best agreement with experiment was obtained for the CI parameters $\epsilon_f = 2.8$ eV ($4f$ binding energy), $U_{ff} = 9.7$ eV (Coulomb repulsion in the $4f$ shell), $V_{\text{eff}} = 0.29$ eV (effective hybridization), and $U_{fc} = 10$ eV (core-hole potential). The ground-state configurational mixing is reliably determined because the four CI parameters are constrained from the energy splittings and intensity ratios [29].

For the analysis of the $M_{4,5}$ XAS data of Ce^{3+} configuration ($3d^{10}4f^1 \rightarrow 3d^9 4f^2$), ionic fm calculations were performed with the atomic Cowan values of the atomic $4f$ ($3d$) spin-orbit interaction reduced to 95% (97%) and the atomic $4f$-$4f$ ($3d$-$4f$) Coulomb repulsion lowered to 60%

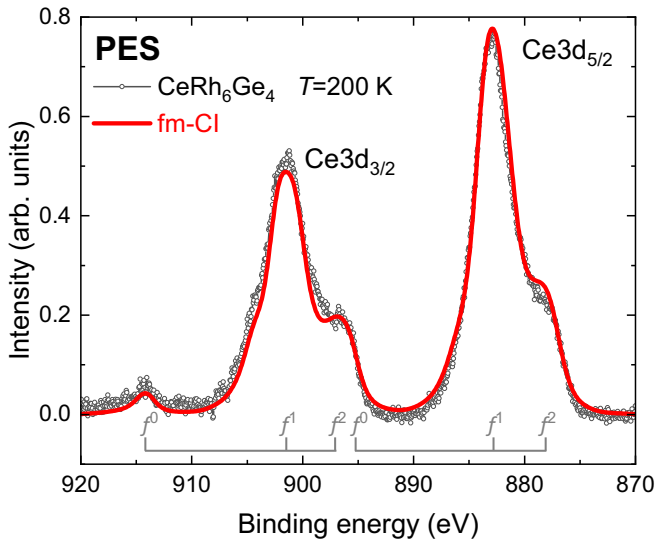


FIG. 1. Ce $3d$ core-level PES data of $CeRh_6Ge_4$ (black circles) after background correction, plus the result of a full-multiplet configuration-interaction (fm-CI) simulation (red line). The gray ruler at the bottom indicates the energy positions of the I(f^n) spectral weights.

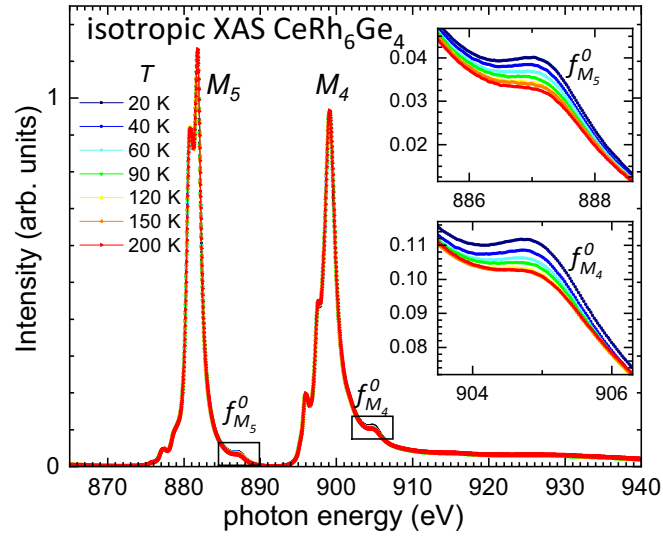


FIG. 2. Isotropic XAS spectra, $I_{iso} = 1/3 \cdot [I(E \parallel c) + 2 \cdot I(E \perp c)]$, of $CeRh_6Ge_4$ at the Ce $M_{4,5}$ edges for several temperatures T between 20 and 200 K. Insets: enlarged view of $4f^0$ satellites at the high-energy tail of the M_5 and M_4 edges.

(80%). The isotropic spectra are constructed from the polarized spectra as $I_{iso} = 1/3 \cdot I(\vec{E} \parallel c) + 2/3 \cdot I(\vec{E} \perp c)$. As discussed in Appendix A, fm calculations of these isotropic spectra agree well with experimental results.

The linear dichroism, LD=I($E \parallel c$)-I($E \perp c$), was calculated for the three pure j_z CEF eigenstates of the Ce^{3+} $J = 5/2$ ground-state multiplet in D_{3h} point symmetry. At low temperatures, this reflects the ground-state orbital occupation, while its temperature dependence is due to thermal occupation of excited CEF states [30]. Deviations from fm calculations are likely due to Kondo-induced mixing of CEF states [31–34]. Notably, the Ce^{4+} $4f^0$ configuration with $J = 0$ does not contribute to the LD.

III. RESULTS AND DISCUSSION

In Fig. 1, the Ce $3d$ core-level PES measurements of $CeRh_6Ge_4$ are shown. The dominant spectral features are assigned to Ce^{3+} $4f^1$ in the initial state. In addition, weaker satellites corresponding to the $4f^0$ and $4f^2$ configurations are observed, indicating a mixed-valence ground state of Ce. The gray rulers at the bottom of the figure indicate the energy positions of the respective $4f^n$ spectral weights. These results provide direct evidence for significant hybridization between the Ce $4f$ states and the conduction electrons in $CeRh_6Ge_4$ and reinforce conclusions from ARPES [18].

To quantitatively assess the degree of hybridization, a fm-CI analysis, as described in Sec. II, was performed. The optimized CI parameters, summarized in Sec. II, yield ground-state configuration weights of 8% $4f^0$, 89% $4f^1$, and 3% $4f^2$, i.e., a total occupation of the $4f$ shell $n_f^{tot} = 0.95$ at 200 K. Comparison with other cerium compounds analyzed within the same simplified fm-CI model suggests that $CeRh_6Ge_4$ is similar to $CeRh_3B_2$ in terms of hybridization strength and configurational mixing [35,36], although the effects are less pronounced in $CeRh_6Ge_4$.

XAS is also sensitive to configuration-interaction effects when the ground state is not purely of $4f^1$ character. Hybridization between the Ce $4f$ and conduction electrons induces a finite $4f^0$ component in the ground (initial) state, giving rise to satellites on the high-energy side of the main Ce^{3+} ($4f^1$) absorption peaks. If these $4f^0$ satellite features originate from Kondo screening, their spectral weight is expected to decrease with increasing temperature.

In Fig. 2, the isotropic XAS spectra of $CeRh_6Ge_4$ are shown for several temperatures between 20 and 200 K. These isotropic spectra are constructed from the measured linear polarized data as described in Sec. II. The $4f^0$ satellites are highlighted by rectangular frames and are displayed on an enlarged scale in the insets. Decreasing spectral weights with increasing temperature are observed, indicative of the Kondo effect, which is consistent with the core-level PES analysis above. Notably, also in XAS the $4f^0$ spectral weights remain pronounced at 200 K.

We now turn to the linearly polarized data. The linearly polarized XAS data of $CeRh_6Ge_4$, measured with $\vec{E} \perp c$ (blue) and $\vec{E} \parallel c$ (red), are shown for all temperatures in Appendix A. Figure 3(a) presents the linearly polarized XAS spectra of $CeRh_6Ge_4$ at 20 K only, together with the experimental linear dichroism LD_{exp} (green). A pronounced polarization dependence is observed.

We first compare the experimental data in Fig. 3(a) qualitatively with simulated polarized XAS spectra for the pure $|\pm j_z\rangle$ states. Figure 3(b) shows the simulation for the M_5 edge, scaled to the experimental data. Both the $|\pm 1/2\rangle$ and $|\pm 3/2\rangle$ states reproduce qualitatively the polarization dependence. However, a direct comparison of the experimental linear dichroism, LD_{exp}, with the simulated dichroism, LD_{j_z}, shown in Fig. 3(c), reveals that $LD_{1/2}$ significantly overestimates while $LD_{3/2}$ underestimates the dichroism.

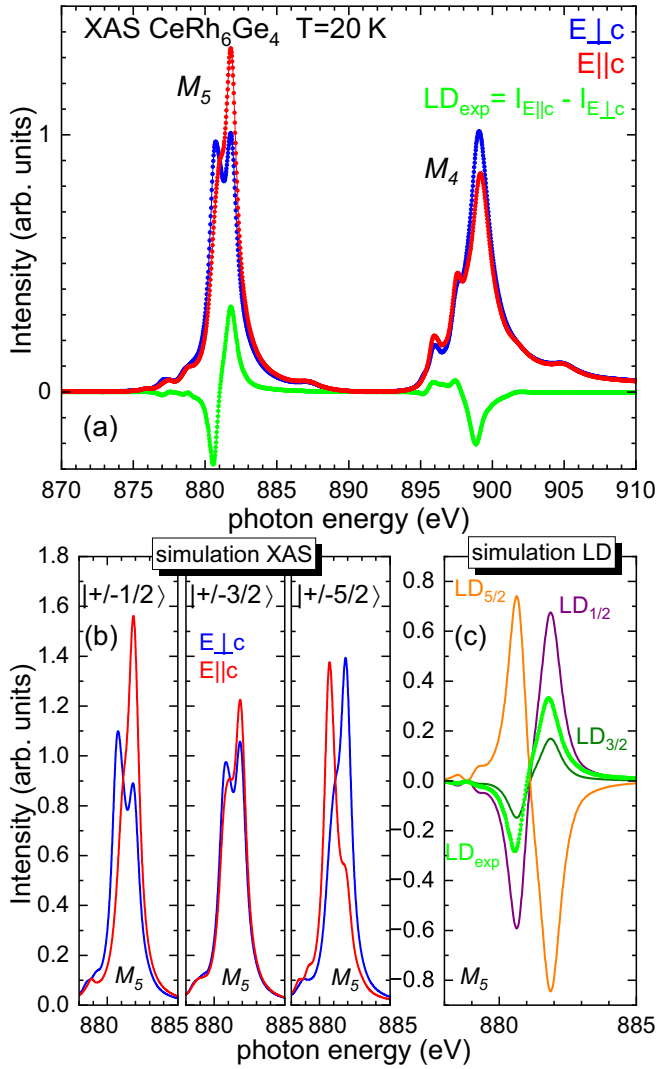


FIG. 3. (a) Linear polarized XAS spectra, I($E \parallel c$) (red) and I($E \perp c$) (blue), of $CeRh_6Ge_4$ at the Ce $M_{4,5}$ edges at $T = 20$ K and the corresponding linear dichroism LD_{exp}=I($E \parallel c$)–I($E \perp c$) (green). (b) Simulated linear polarized XAS spectra of pure $|\pm j_z\rangle$ states. (c) Simulated linear dichroism of pure $|\pm j_z\rangle$ states, LD_{jz}, compared to experimental LD_{exp} [green dotted curve taken from (a)].

We recall that the $LD_{1/2}$ state is expected to form the ground state and that, keeping in mind thermal population of the CEF levels, its occupation at 20 K should be approximately 95%, while the $|\pm 3/2\rangle$ state at 5.8 meV should contribute about 5% [see the dashed lines in Fig. 4(d)]. It is evident that the CEF scheme considered here, including the thermal population of excited states, cannot reproduce the experimentally observed dichroism at 20 K. However, the low-temperature dichroism can be reproduced either by assuming a $|\pm 1/2\rangle$ ground state with a $|\pm 5/2\rangle$ excited state close in energy and partially populated, or by considering a $|\pm 3/2\rangle$ ground state with partial thermal population of a $|\pm 1/2\rangle$ excited state, but both scenarios are inconsistent with the anisotropy of the static magnetic susceptibility and, in the latter case, the experimentally observed in-plane alignment of the ordered moments.

Figure 4(a) shows the temperature dependence of the experimental linear dichroism, $LD_{exp}(T)$. The dichroism decreases continuously between 20 and 200 K, from $LD_{exp}(20\text{ K}) = 0.33$ to $LD_{exp}(200\text{ K}) = 0.22$ (arbitrary units in our normalization), as measured at the energy of the maximum $LD_{exp}(T)$ at the M_5 edge. This continuous decrease of $LD_{exp}(T)$ with increasing temperature confirms the sequence of CEF states, with the $|\pm 1/2\rangle$ lowest in energy and the $|\pm 5/2\rangle$ highest. By contrast, if a $|\pm 5/2\rangle$ were close in energy to the $|\pm 1/2\rangle$ ground state, the *LD* would change sign upon increasing temperature. Likewise, if the $|\pm 3/2\rangle$ state were lowest in energy, the *LD* would initially increase as the $|\pm 1/2\rangle$ becomes thermally populated, before decreasing as the $|\pm 5/2\rangle$ state becomes increasingly populated. Hence, the temperature dependence of $LD_{exp}(T)$ independently confirms the sequence of CEF states deduced from the analysis of the static susceptibility [21].

The temperature dependence of the dichroism was then calculated by quantitatively accounting only for thermal occupation of CEF states using the CEF scheme proposed in Ref. [21]. The calculated dichroism is shown in Fig. 4(b). The dashed lines in Fig. 4(d) indicate the corresponding thermal populations of the CEF levels. As expected from the qualitative comparison above, the calculated dichroism at 20 K is significantly overestimated. It amounts to 0.66 at 20 K and 0.28 at 200 K in the same normalization. Thus, while the calculated value is in reasonable agreement with experiment at 200 K, it exceeds the experimental dichroism at low temperatures by approximately a factor of 2.

The lack of reproducibility of LD_{exp} is reminiscent of the case observed in another ferromagnetic Kondo system, hexagonal $CeRh_3B_2$. In $CeRh_3B_2$, the $|\pm 1/2\rangle$ is also the lowest-energy CEF level, giving rise to an in-plane ordered magnetic moment that is strongly reduced [36,37]. In this compound, the experimentally observed LD_{exp} is likewise smaller than the *LD* calculated for a pure $|\pm 1/2\rangle$ state [33]. Furthermore, $CeRh_3B_2$ exhibits, like $CeRh_6Ge_4$, a seemingly contradictory set of observations indicative of a large Kondo temperature of several hundred Kelvin [35,38–45] despite its high magnetic ordering temperature [36,37]. This behavior has been explained in terms of a multiorbital ground state, consisting of the $|\pm 1/2\rangle$ component responsible for the magnetic order, and admixed higher-lying CEF states that hybridize strongly with the conduction electrons and give rise to the Kondo effect [33].

In the following, a similar multiorbital scenario is investigated for $CeRh_6Ge_4$ using a simplified Anderson impurity model (SIAM) to calculate the occupation of the CEF states for a finite Kondo temperature and a total $4f$ shell occupation $n_f^{tot} < 1$. SIAM, treated within the noncrossing approximation (NCA) [46–48], accounts for the hybridization of the three CEF states with the conduction-electrons bath. Such a multiorbital ground state can generally occur when the Kondo energy scale and CEF splittings are comparable, as in, e.g., $CeRh_3B_2$ [33], $CeRh_4Sn_6$ [31,32] or $CeRh_2As_2$ [34]. The present calculations are based on the assumption of isotropic hybridization, whereby all CEF states are assumed to couple equally to the conduction-electron bath. In reality, however, symmetry considerations suggest that CEF states of different symmetry generally hybridize with different strengths.

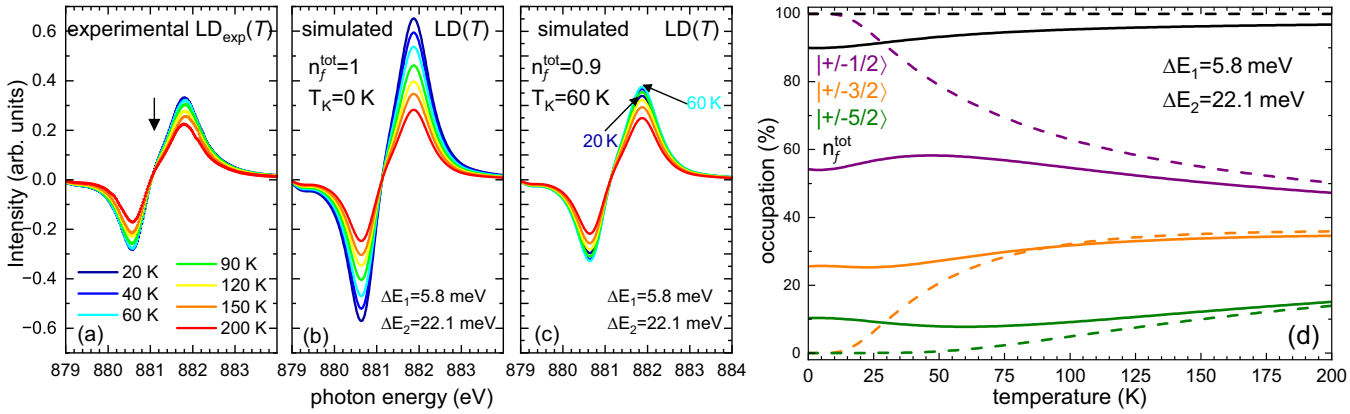


FIG. 4. (a) Temperature dependence of the experimental linear dichroism, $LD_{\rm exp}(T)$. (b) Simulated $LD(T)$ based on thermal occupation of states using the CEF model as described in the text, corresponding to $T_K = 0$ K and $n_f^{\rm tot}(T) = 1$. (c) Simulated $LD(T)$ taking into account the Kondo effect in addition to thermal occupation of states; see the text. (d) Occupation of states as a function of temperature for pure thermal occupation (dashed lines) and in the presence of the Kondo effect with $T_K = 60$ K and $n_f^{\rm tot}(T = 0) = 0.9$ (solid lines). The black lines are the total occupation $n_f^{\rm tot}(T)$ of the $4f$ shell with (solid) and without (dashed) the Kondo effect. In the $T = 0$ K limit, 35% of the $4f$ shell occupancy is due to $|\pm 3/2\rangle$ and $|\pm 5/2\rangle$ states.

The SIAM/NCA calculations, assuming the same CEF model as above, were performed for $n_f^{\rm tot} = 0.9$ at $T = 0$ K, as this value corresponds well to $n_f^{\rm tot} \approx 0.95$ at 200 K as deduced from the analysis of the core-level data [see the solid black line in Fig. 4(d)]. Calculations taking Kondo temperatures ranging from 0 to 190 K found that $T_K = 60$ K provided the best overall agreement with experimentally determined LD. The Kondo effect induces a finite occupation of the excited CEF states even at $T = 0$ K as demonstrated in Fig. 4(d) by the solid lines. As a consequence, the partial occupation of the $|\pm 5/2\rangle$, which exhibits a large dichroism of opposite sign [see Fig. 3(c)], strongly reduces the simulated LD at low temperatures. The resulting Kondo-mixed ground state reproduces $LD_{\rm exp}$ at 20 K reasonably well [see Fig. 4(c)]. Furthermore, the experimental dichroism at 200 K is well reproduced, as at this temperature the influence of the Kondo effect is strongly reduced and the occupations of the CEF states closely resemble those expected from purely thermal population in the absence of the Kondo effect.

However, a minor shortcoming is the initial increase of the simulated LD. [For example, compare the relative maxima at 20 and 60 K in experimental data, Fig. 4(a), and the simulation, Fig. 4(c).] This small discrepancy arises from the initially decreasing occupation of the excited states with increasing temperature due to the diminishing impact of the Kondo effect as temperature rises [see Fig. 4(d)]. For even higher temperatures, thermal occupation becomes important, leading to a decrease of LD. If the Kondo temperature of the excited $|\pm 5/2\rangle$ state were higher than that of the $|\pm 1/2\rangle$, the influence of the Kondo effect would persist to higher temperatures, and this nonmonotonic behavior of the LD could potentially be avoided. However, different Kondo hybridization strengths for the individual CEF states are not included in the present model.

A multiorbital ground state with contributions from $|\pm 3/2\rangle$ and $|\pm 5/2\rangle$, each having a different, and possibly stronger, hybridization than the $|\pm 1/2\rangle$ component, accounts for the discrepancy between a Kondo temperature deduced from specific heat C ($T_K^C \sim 20$ K) under the assumption of a spin-1/2 ground state [9] and a broad spin response found in inelastic neutron scattering [21]. For example, the INS data cannot be described using the crystal-field model derived from static susceptibility together with an intrinsic line broadening corresponding to the Kondo temperature obtained from specific heat. Instead, the INS data are consistent with a Kondo temperature of ∼60 K. This is demonstrated in Appendix B, where calculations of the imaginary part of the dynamical susceptibility and corresponding structure factors of $CeRh_6Ge_4$ are presented within the framework of the present Anderson impurity model, thereby explicitly taking into account the multiorbital nature of the ground state.

A multiorbital ground state is also implied from a Kadowaki-Woods ratio close to that expected for a fourfold-degenerate ground state [11]. To give the measured Sommerfeld coefficient, in this limit T_K should be about three times larger than expected for an effective $S = 1/2$ state, i.e., $T_K \sim 60$ K [49]. This same value of $T_K \sim 60$ K, determined independently in our SIAM/NCA calculations of LD, also accounts for the magnitude and general temperature dependence of $LD_{\rm exp}(T)$. Given approximations in both determinations of T_K, it is not possible to say that the ground state is fourfold-degenerate, but it clearly is effectively greater than doubly degenerate due to multiorbital contributions.

In SIAM/NCA calculations, the Kondo hybridization was taken to be orbital-independent, but there is already evidence of a Kondo effect at 200 K in the core-level PES as well as XAS data (Figs. 1 and 2), which is well above $T_K \sim 60$ K resulting from an orbital averaged hybridization and which is comparable to the energy of the highest-lying CEF doublet. Though ARPES was performed only to 120 K, these measurements also revealed clear evidence of f-c hybridization and its anisotropy at 120 K [18]. Thus, both XAS and (AR)PES argue for a Kondo effect on the $|\pm 5/2\rangle$ CEF level with a characteristic temperature greater than the orbital-average

T_K. As mentioned, a stronger hybridization of the $|\pm 5/2\rangle$ level would improve agreement between experiment and the calculated temperature dependence of the LD.

Though the $|\pm 1/2\rangle$ orbital dictates in-plane ordered moments, Kondo-derived mixing of higher-lying CEF levels into the ground state plays a role in reducing the magnitude of the ordered moment and the f-shell occupation. It is not surprising, then, that angle-dependent de Haas–van Alphen measurements give a Fermi surface topology that has both localized and itinerant $4f$ characters found in LDA + U band calculations, but the Fermi volume is more characteristic of the $4f$-localized limit [17], which supports a Kondo-breakdown interpretation of quantum criticality in $CeRh_6Ge_4$ [11]. Duality in $4f$ character arising from multiorbital mixing does not rule out this view of criticality; however, it leaves open alternative interpretations of its origin [16,19].

The pressure dependence of crystal fields may play a role in an alternative interpretation [19]. Results presented here argue that this suggestion might merit more attention, particularly because Kondo and CEF energy scales in $CeRh_6Ge_4$ are comparable. Typically, the Kondo scale in Ce-based Kondo systems is strongly volume-dependent and gives a dominant, low-temperature contribution to a large Gruneissen parameter. The CEF splitting is also volume-dependent but much less so in the absence of a Kondo effect in the higher-lying CEF states [50]. As we have discussed, charge and magnetic spectroscopies, however, do show the presence of a Kondo effect in these CEF states, and therefore the measured Gruneissen parameter is a mixture of both contributions with the CEF-derived Gruneissen parameter making a more significant contribution, even at temperatures well below the first excited CEF level. Such a CEF contribution could influence an interpretation of the diverging temperature dependence of the Gruneissen parameter of $CeRh_6Ge_4$ as it is tuned to a QCP [16].

IV. SUMMARY

In summary, core-level PES and isotropic XAS measurements provide clear evidence of a temperature-dependent $4f^0$ contribution to the electronic spectrum of $CeRh_6Ge_4$ that persists to at least 200 K, even at atmospheric pressure. Linearly polarized XAS reveals a temperature-dependent linear dichroism consistent with the sequence of CEF states inferred from the static susceptibility, $|\pm 1/2\rangle$, $|\pm 3/2\rangle$, and $|\pm 5/2\rangle$. The experimental dichroism cannot be reproduced by an ionic full-multiplet model alone, but is captured when the Kondo effect is included, assuming a total $4f$-shell occupation of 0.9 and an orbital-independent Kondo temperature of 60 K resulting from orbital-independent hybridization. This value of T_K is also consistent with a quasiquartet ground state inferred from thermodynamic and transport measurements. The detailed temperature dependence of the linear dichroism, however, deviates from that expected for isotropic hybridization, suggesting stronger hybridization for the excited CEF states. This suggestion aligns with conclusions from ARPES and neutron scattering experiments. Importantly, the Kondo effect induces nontrivial contributions of both first and second excited crystal-field doublets into the ground state. The resulting multiorbital ground state should be considered the starting point for a model of pressure-induced criticality. Our experiments do not rule out a Kondo-breakdown interpretation of quantum criticality in $CeRh_6Ge_4$, but they do leave open alternative scenarios and in particular highlight the possible role of crystal fields in an interpretation.

ACKNOWLEDGMENTS

We thank Z. Riedel for sharing the results of his specific-heat measurements on $CeRh_6Ge_4$ and $LaRh_6Ge_4$. A.S. acknowledges support from the German Research Foundation (DFG), Grant No. 567326535. Work at Los Alamos National Laboratory was performed under the auspices of the U.S. Department of Energy, Office of Basic Energy Sciences, Division of Materials Science and Engineering under project "Quantum Fluctuations in Narrow-Band Systems." All authors acknowledge the support from the Max Planck-POSTECH-Hsinchu Center for Complex Phase Materials.

DATA AVAILABILITY

The data that support the findings of this article are not publicly available. The data are available from the authors upon reasonable request.

APPENDIX A: ISOTROPIC AND DIRECTIONAL DEPENDENT XAS SPECTRA

Figure 5 shows the agreement between our isotropic simulation and XAS data. The small satellites at 887 and 905 eV are not reproduced, as they arise from the Ce^{4+} configuration in the ground state and correspond to the transition $(3d^{10}4f^0 \rightarrow 3d^9 4f^1)$, which is not accounted for in the ionic calculation.

Due to geometrical constraints in the experiment, measurements with $\vec{E} \parallel c$ could not be realized. Instead, the spectra were recorded with $\vec{E} \parallel \tilde{c}$, where $\tilde{c}$ is tilted by 20° with respect to the crystallographic c direction. Within the dipole limit of XAS in D_{3h} point symmetry, the $\vec{E} \parallel c$ spectrum

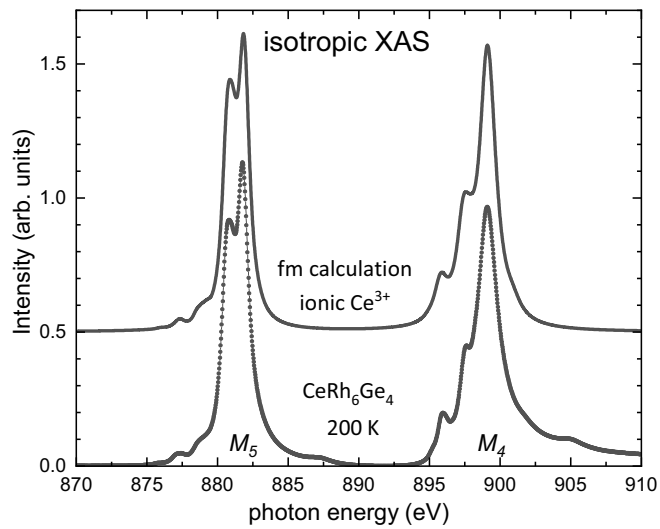


FIG. 5. Isotropic XAS spectra at the Ce $M_{4,5}$ edges of $CeRh_6Ge_4$ at 200 K constructed from linear polarized data based on Eq. (A1) and full-multiplet (fm) calculation for Ce^{3+} (top).

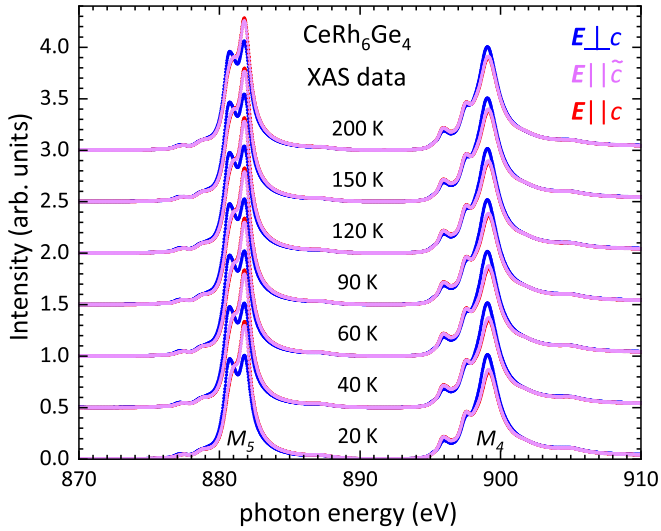


FIG. 6. Linearly polarized XAS spectra of $CeRh_6Ge_4$ at various temperature for the electric field vector $\vec{E} \perp c$ (blue) and $\vec{E} \parallel \tilde{c}$ (pink) with $\tilde{c}$ 20° off the crystallographic c direction. The spectra $\vec{E} \parallel c$ (red) were reconstructed following Eq. (A1).

can nevertheless be reconstructed as a linear combination of $\vec{E} \parallel \tilde{c}$ and $\vec{E} \perp c$ according to the relation

$$I(\vec{E} \parallel \tilde{c}) = \cos^2(20^\circ) \cdot I(\vec{E} \parallel c) + \sin^2(20^\circ) \cdot I(\vec{E} \perp c). \tag{A1}$$

Figure 6 shows the measured XAS spectra for $\vec{E} \perp c$ and $\vec{E} \parallel \tilde{c}$, together with the reconstructed $\vec{E} \parallel c$, at several temperatures between 20 and 200 K. The latter differs noticeably only in the energy regions where the *LD* is large. Accordingly, the isotropic spectrum shown in Fig. 5 is given by $I_{iso} \approx 0.38 \cdot I(\vec{E} \parallel \tilde{c}) + 0.62 \cdot I(\vec{E} \perp c)$, and the *LD*, $I(\vec{E} \parallel c)$-$I(\vec{E} \perp c)$, is approximately 13% larger than the difference between the measured spectra, $I(\vec{E} \parallel \tilde{c})$-$I(\vec{E} \perp c)$.

APPENDIX B: IMAGINARY PART OF DYNAMICAL SUSCEPTIBILITY AND STRUCTURE FACTOR

The INS data of $CeRh_6Ge_4$ are not compatible with the line broadening expected for the specific-heat-derived Kondo temperature of 20 K nor with a Kondo temperature well above 100 K, as the width of the high-energy tail in the neutron data may suggest [21].

In the following, the dynamical susceptibility $\mathrm{Im}\,\chi(\omega, T)$ and the corresponding structure factor are calculated for the following parameters:

(1) Kondo temperature $T_K = 60$ K.
(2) Low-temperature $4f$-valence $n_f(T = 0) = 0.9$.
(3) CEF scheme (see Table I).

TABLE I. CEF states and excitation energies.

State	Energy (meV)	Energy (K)
$\lvert\pm\frac{1}{2}\rangle$	0	0
$\lvert\pm\frac{3}{2}\rangle$	5.8	67.3
$\lvert\pm\frac{5}{2}\rangle$	22.1	256.5

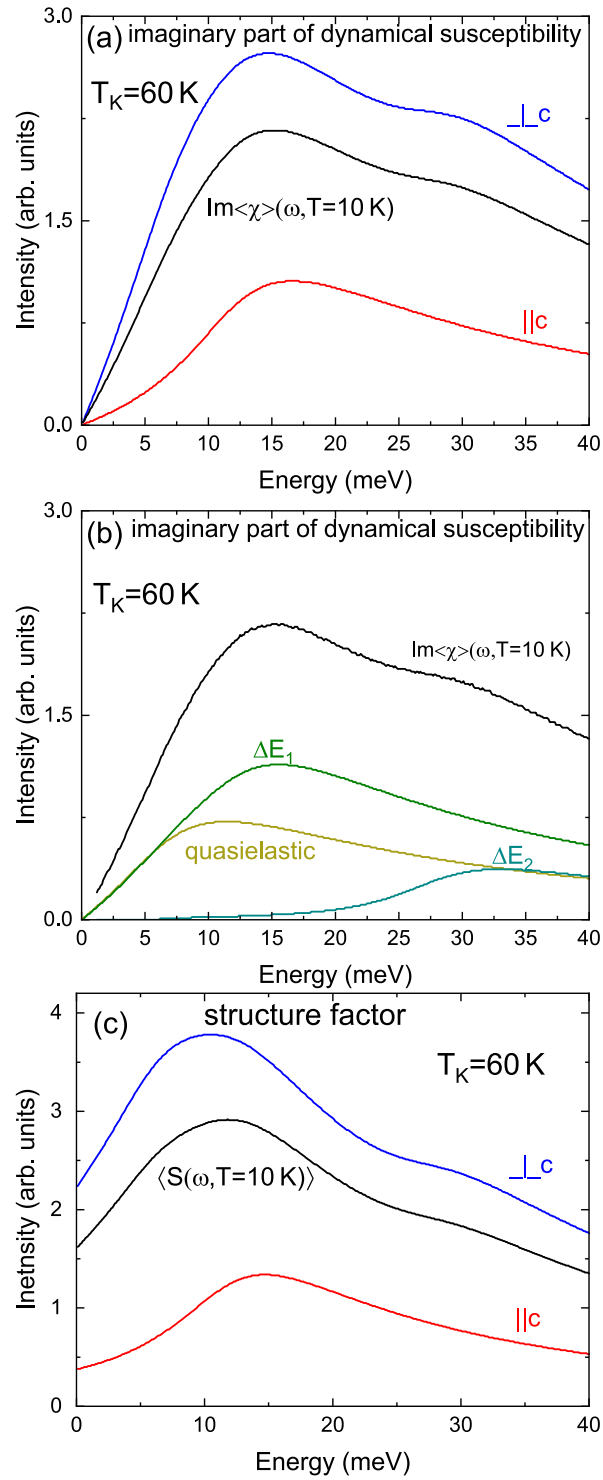


FIG. 7. Calculated spin response of $CeRh_6Ge_4$: Directional dependence (a) and spectral contributions (b) of the imaginary part of the dynamical susceptibility $\mathrm{Im}\,\langle\chi(\omega, T)\rangle$ and corresponding structure factor $\langle S(\omega, T)\rangle$ (c).

(4) Hybridization strength:

The *isotropic* hybridization strength is adjusted so as to reproduce the low-temperature $4f$-valence.

As a result of Kondo-singlet formation, f-contributions from the excited CEF states are mixed into the ground state.

For isotropic hybridization, the relative weights of these contributions depend upon the ratio of the Kondo temperature and the CEF excitation energies. In the resulting multiorbital ground state, with contributions of $|\pm\frac{1}{2}\rangle$, $|\pm\frac{3}{2}\rangle$, and $|\pm\frac{5}{2}\rangle$ as in Fig. 4(d), the dipole selection rules for INS allow transitions not only from the ground state to the first excited state at 5.8 meV, but also to the second excited state at 22.1 meV. Furthermore, the excitation energies appear shifted by the Kondo temperature, i.e., $\Delta E_{\mathrm{CEF}} + T_K$.

We show the dynamical susceptibilities $\mathrm{Im}\,\chi_{\perp c}(\omega, T)$, $\mathrm{Im}\,\chi_{\parallel c}(\omega, T)$, and the orientationally averaged $\mathrm{Im}\,\langle\chi(\omega, T)\rangle = \mathrm{Im}\,[\frac{2}{3}\chi_{\perp c}(\omega, T) + \frac{1}{3}\chi_{\parallel c}(\omega, T)]$ in Fig. 7(a) as well as the respective contributions from the Kondo ground state (quasielastic) and van Vleck terms (ΔE_1 and ΔE_2) in Fig. 7(b), all for isotropic hybridization. The corresponding structure factors $\langle S(\omega, T)\rangle$ are shown in Fig. 7(c). In the Kondo regime, the calculated structure factor reproduces the characteristic features of the INS data quite well [21], namely a rather broad peak around 10 meV, a slight bump between 20 and 30 meV, and an extended high-energy tail. The latter is a consequence of Kondo-induced broadening.

[1] D. Belitz, T. R. Kirkpatrick, and T. Vojta, First order transitions and multicritical points in weak itinerant ferromagnets, Phys. Rev. Lett. **82**, 4707 (1999).

[2] A. V. Chubukov, C. Pépin, and J. Rech, Instability of the quantum-critical point of itinerant ferromagnets, Phys. Rev. Lett. **92**, 147003 (2004).

[3] D. Belitz, T. R. Kirkpatrick, and T. Vojta, How generic scale invariance influences quantum and classical phase transitions, Rev. Mod. Phys. **77**, 579 (2005).

[4] G. J. Conduit, A. G. Green, and B. D. Simons, Inhomogeneous phase formation on the border of itinerant ferromagnetism, Phys. Rev. Lett. **103**, 207201 (2009).

[5] M. Brando, D. Belitz, F. M. Grosche, and T. R. Kirkpatrick, Metallic quantum ferromagnets, Rev. Mod. Phys. **88**, 025006 (2016).

[6] T. R. Kirkpatrick and D. Belitz, Ferromagnetic quantum critical point in noncentrosymmetric systems, Phys. Rev. Lett. **124**, 147201 (2020).

[7] A. Steppke, R. Küchler, S. Lausberg, E. Lengyel, L. Steinke, R. Borth, T. Lühmann, C. Krellner, M. Nicklas, C. Geibel, F. Steglich, and M. Brando, Ferromagnetic quantum critical point in the heavy-fermion metal $YbNi_4(P_{1-x}As_x)_2$, Science **339**, 933 (2013).

[8] D. Voßwinkel, O. Niehaus, U. C. Rodewald, and R. Pöttgen, Bismuth flux growth of $CeRh_6Ge_4$ and $CeRh_2Ge_2$ single crystals, Z. Naturforsch. B **67**, 1241 (2012).

[9] E. Matsuoka, C. Hondo, T. Fujii, A. Oshima, H. Sugawara, T. Sakurai, H. Ohta, F. Kneidinger, L. Salamakha, H. Michor, and E. Bauer, Ferromagnetic transition at 2.5 K in the hexagonal Kondo-lattice compound $CeRh_6Ge_4$, J. Phys. Soc. Jpn. **84**, 073704 (2015).

[10] H. Kotegawa, E. Matsuoka, T. Uga, M. Takemura, M. Manago, N. Chikuchi, H. Sugawara, H. Tou, and H. Harima, Indication of ferromagnetic quantum critical point in Kondo lattice $CeRh_6Ge_4$, J. Phys. Soc. Jpn. **88**, 093702 (2019).

[11] B. Shen, Y. Zhang, Y. Komijani, M. Nicklas, R. Borth, A. Wang, Y. Chen, Z. Nie, R. Li, X. Lu, H. Lee, M. Smidman, F. Steglich, P. Coleman, and H. Yuan, Strange-metal behaviour in a pure ferromagnetic Kondo lattice, Nature (London) **579**, 51 (2020).

[12] S. Paschen and Q. Si, Quantum phases driven by strong correlations, Nat. Rev. Phys. **3**, 9 (2020).

[13] Y. Komijani and P. Coleman, Model for a ferromagnetic quantum critical point in a 1d Kondo lattice, Phys. Rev. Lett. **120**, 157206 (2018).

[14] S. Shin, A. Ramires, V. Pomjakushin, I. Plokhikh, and E. Pomjakushina, Ferromagnetic quantum critical point protected by nonsymmorphic symmetry in a Kondo metal, Nat. Commun. **15**, 8423 (2024).

[15] S. J. Yamamoto and Q. Si, Metallic ferromagnetism in the Kondo lattice, Proc. Natl. Acad. Sci. USA **107**, 15704 (2010).

[16] J. Zhan, Y. Zhang, J. Zhang, Y. Liu, Z. Nie, Y. Chen, L. Jiao, Y. Komijani, M. Smidman, F. Steglich, P. Coleman, and H. Yuan, Critical fluctuations and conserved dynamics in a strange ferromagnetic metal, Phys. Rev. Lett. **135**, 266504 (2025).

[17] A. Wang, F. Du, Y. Zhang, D. Graf, B. Shen, Y. Chen, Y. Liu, M. Smidman, C. Cao, F. Steglich, and H. Yuan, Localized 4f-electrons in the quantum critical heavy fermion ferromagnet $CeRh_6Ge_4$, Sci. Bull. **66**, 1389 (2021).

[18] Y. Wu, Y. Zhang, F. Du, B. Shen, H. Zheng, Y. Fang, M. Smidman, C. Cao, F. Steglich, H. Yuan, J. D. Denlinger, and Y. Liu, Anisotropic c-f hybridization in the ferromagnetic quantum critical metal $CeRh_6Ge_4$, Phys. Rev. Lett. **126**, 216406 (2021).

[19] S. M. Thomas, S. Seo, T. Asaba, F. Ronning, P. F. S. Rosa, E. D. Bauer, and J. D. Thompson, Probing quantum criticality in ferromagnetic $CeRh_6Ge_4$, Phys. Rev. B **109**, L121105 (2024).

[20] S. Itokazu, A. Kirikoshi, H. O. Jeschke, and J. Otsuki, From localized 4f electrons to anisotropic exchange interactions in ferromagnetic $CeRh_6Ge_4$, Commun. Mater. **6**, 269 (2025).

[21] J. W. Shu, D. T. Adroja, A. D. Hillier, Y. J. Zhang, Y. X. Chen, B. Shen, F. Orlandi, H. C. Walker, Y. Liu, C. Cao, F. Steglich, H. Q. Yuan, and M. Smidman, Magnetic order and crystalline electric field excitations of the quantum critical heavy-fermion ferromagnet $CeRh_6Ge_4$, Phys. Rev. B **104**, L140411 (2021).

[22] R. Yamamoto, S. Park, Z. W. Riedel, P. Sherpa, J. D. Thompson, F. Ronning, E. D. Bauer, A. P. Dioguardi, and M. Hirata, Evidence for easy-plane xy ferromagnetism in heavy-fermion quantum-critical $CeRh_6Ge_4$, Phys. Rev. B **112**, 155152 (2025).

[23] M. W. Haverkort, *Quanty* for core level spectroscopy - excitons, resonances and band excitations in time and frequency domain, J. Phys.: Conf. Ser. **712**, 012001 (2016).

[24] J.-M. Imer and E. Wuilloud, A simple model calculation for XPS, BIS and EELS 4f-excitations in Ce and La compounds, Z. Phys. B **66**, 153 (1987).

[25] R. Cowan, *The Theory of Atomic Structure and Spectra* (University of California, Berkeley, CA, 1981).

[26] A. Tanaka, and T. Jo, Resonant 3d, 3p and 3s photoemission in transition metal oxides predicted at 2p threshold, J. Phys. Soc. Jpn. **63**, 2788 (1994).

[27] F. de Groot and A. Kotani, *Core Level Spectrocopy of Solids*, Advances in Condensed Matter Science (CRC, Boca Raton, FL, 2008), Vol. 6.

[28] F. Strigari, M. Sundermann, Y. Muro, K. Yutani, T. Takabatake, K.-D. Tsuei, Y. Liao, A. Tanaka, P. Thalmeier, M. Haverkort, L. Tjeng, and A. Severing, Quantitative study of valence and configuration interaction parameters of the Kondo semiconductors CeM_2Al_{10} (M=Ru, Os and Fe) by means of bulk-sensitive hard x-ray photoelectron spectroscopy, J. Electron Spectrosc. Relat. Phenom. **199**, 56 (2015).

[29] O. Gunnarsson and K. Schönhammer, Electron spectroscopies for Ce compounds in the impurity model, Phys. Rev. B **28**, 4315 (1983).

[30] P. Hansmann, A. Severing, Z. Hu, M. W. Haverkort, C. F. Chang, S. Klein, A. Tanaka, H. H. Hsieh, H.-J. Lin, C. T. Chen, B. Fåk, P. Lejay, and L. H. Tjeng, Determining the crystal-field ground state in rare earth heavy fermion materials using soft-x-ray absorption spectroscopy, Phys. Rev. Lett. **100**, 066405 (2008).

[31] M. Sundermann, F. Strigari, T. Willers, H. Winkler, A. Prokofiev, J. M. Ablett, J.-P. Rueff, D. Schmitz, E. Weschke, M. M. Sala, A. Al-Zein, A. Tanaka, M. W. Haverkort, D. Kasinathan, L. H. Tjeng, S. Paschen, and A. Severing, $CeRu_4Sn_6$: A strongly correlated material with nontrivial topology, Sci. Rep. **5**, 17937 (2015).

[32] P. Wissgott and K. Held, Electronic structure of $CeRu_4Sn_6$: A density functional plus dynamical mean field theory study, Eur. Phys. J. B **89**, 5 (2016).

[33] A. Amorese, P. Hansmann, A. Marino, P. Körner, T. Willers, A. Walters, K.-J. Zhou, K. Kummer, N. B. Brookes, H.-J. Lin, C.-T. Chen, P. Lejay, M. W. Haverkort, L. H. Tjeng, and A. Severing, Orbital selective coupling in $CeRh_3B_2$: Coexistence of high Curie and high Kondo temperatures, Phys. Rev. B **107**, 115164 (2023).

[34] D. S. Christovam, M. Ferreira-Carvalho, A. Marino, M. Sundermann, D. Takegami, A. Melendez-Sans, K. D. Tsuei, Z. Hu, S. Rößler, M. Valvidares, M. W. Haverkort, Y. Liu, E. D. Bauer, L. H. Tjeng, G. Zwicknagl, and A. Severing, Spectroscopic evidence of Kondo-induced quasiquartet in $CeRh_2As_2$, Phys. Rev. Lett. **132**, 046401 (2024).

[35] M. Sundermann, F. Strigari, T. Willers, J. Weinen, Y. Liao, K.-D. Tsuei, N. Hiraoka, H. Ishii, H. Yamaoka, J. Mizuki, Y. Zekko, E. Bauer, J. Sarrao, J. Thompson, P. Lejay, Y. Muro, K. Yutani, T. Takabatake, A. Tanaka, N. Hollmann, *et al.*, Quantitative study of the f occupation in $CeMIn_5$ and other cerium compounds with hard x-rays, J. Electron Spectrosc. Relat. Phenom. **209**, 1 (2016).

[36] S. K. Dhar, S. K. Malik, and R. Vijayaraghavan, Strong itinerant magnetism in ternary boride $CeRh_3B_2$, J. Phys. C **14**, L321 (1981).

[37] A. Galatanu, E. Yamamoto, T. Okubo, M. Yamada, A. Thamizhavel, T. Takeuchi, K. Sugiyama, Y. Inada, and Y. Onuki, On the unusual magnetic behaviour of $CeRh_3B_2$, J. Phys.: Condens. Matter **15**, S2187 (2003).

[38] S. Malik, R. Vijayaraghavan, W. Wallace, and S. Dhar, Magnetic behavior of R_3B_2 (R = La to Gd) ternary borides, J. Magn. Magn. Mater. **37**, 303 (1983).

[39] M. Maple, S. Lambert, M. Torikachvili, K. Yang, J. Allen, B. Pate, and I. Lindau, Superconductivity, magnetism and valence fluctuations in rare earth-transition metal borides, J. Less-Common Met. **111**, 239 (1985).

[40] Y. Kitaoka, Y. Kishimoto, K. Asayama, T. Kohara, K. Takeda, R. Vijayaraghavan, S. Malik, S. Dhar, and D. Rambabu, Magnetic behavior of $RERh_3B_2$ (RE = La, Ce, Nd, and Gd), J. Magn. Magn. Mater. **52**, 449 (1985).

[41] E. V. Sampathkumaran, G. Kaindl, C. Laubschat, W. Krone, and G. Wortmann, Spectroscopic evidence against Rh 4d itinerant ferromagnetism in $CeRh_3B_2$, Phys. Rev. B **31**, 3185 (1985).

[42] S. A. Shaheen, J. S. Schilling, and R. N. Shelton, Anomalous ferromagnetism in $CeRh_3B_2$: Possibility of a new Kondo-lattice state, Phys. Rev. B **31**, 656 (1985).

[43] A. Fujimori, T. Takahashi, A. Okabe, M. Kasaya, and T. Kasuya, Photoemission study of the ferromagnetic Kondo system $CeRh_3B_2$, Phys. Rev. B **41**, 6783 (1990).

[44] J. W. Allen, M. B. Maple, J.-S. Kang, K. N. Yang, M. S. Torikachvili, Y. Lassailly, W. P. Ellis, B. B. Pate, and I. Lindau, Density-of-states-driven transition from superconductivity to ferromagnetism in $CeRh_3B_2$: Scenario for an exchange-split Kondo resonance, Phys. Rev. B **41**, 9013 (1990).

[45] T. Takeuchi, A. Thamizhavel, T. Okubo, M. Yamada, Y. Inada, A. Galatanu, E. Yamamoto, and Y. Ōnuki, Thermal expansion and magnetostriction in $CeRh_3B_2$, J. Magn. Magn. Mater. **272–276**, E17 (2004), proceedings of the International Conference on Magnetism (ICM 2003).

[46] V. Zevin, G. Zwicknagl, and P. Fulde, Temperature dependence of the $4f$ quadrupole moment of Yb in YbCu2Si$_2$, Phys. Rev. Lett. **60**, 2331 (1988).

[47] G. Zwicknagl, V. Zevin, and P. Fulde, Simple approximation scheme for the Anderson impurity Hamiltonian, Z. Phys. B **79**, 365 (1990).

[48] A. Amorese, A. Marino, M. Sundermann, K. Chen, Z. Hu, T. Willers, F. Choueikani, P. Ohresser, J. Herrero-Martin, S. Agrestini, C. T. Chen, H.-J. Lin, M. W. Haverkort, S. Seiro, C. Geibel, F. Steglich, L. H. Tjeng, G. Zwicknagl, and A. Severing, Possible multiorbital ground state in $CeCu_2Si_2$, Phys. Rev. B **102**, 245146 (2020).

[49] V. T. Rajan, Magnetic susceptibility and specific heat of the Coqblin-Schrieffer model, Phys. Rev. Lett. **51**, 308 (1983).

[50] J. D. Thompson and J. M. Lawrence, *Handbook on the Physics and Chemistry of Rare Earths* (Elsevier, Amsterdam, 1994), p. 383.